Accepted Manuscript

Assessment of calcium addition on the removal of U(VI) in the alkaline conditions created by NH_3 gas

Yelena Katsenovich, Claudia Cardona, Jim Szecsody, Leonel Lagos, Walter Tang

PII: S0883-2927(18)30054-4

DOI: 10.1016/j.apgeochem.2018.03.003

Reference: AG 4051

To appear in: *Applied Geochemistry*

Received Date: 27 June 2017

Revised Date: 24 February 2018

Accepted Date: 2 March 2018

Please cite this article as: Katsenovich, Y., Cardona, C., Szecsody, J., Lagos, L., Tang, W., Assessment of calcium addition on the removal of U(VI) in the alkaline conditions created by NH_3 gas, *Applied Geochemistry* (2018), doi: 10.1016/j.apgeochem.2018.03.003.

Assessment of Calcium Addition on the Removal of U(VI) in the Alkaline Conditions Created by NH_3 Gas

Yelena Katsenovich[a*], Claudia Cardona[a,b], Jim Szecsody[c], Leonel Lagos[a], Walter Tang[b]

[a] Applied Research Center, [b] Department of Civil and Environmental Engineering, Florida International University, 10555 W. Flagler Street, Miami, FL 33174, USA

[c] Pacific Northwest National Laboratory, PO Box 999, K3-62, Richland, WA 99352

*Corresponding author:
katsenov@fiu.edu

Abstract

Remediation of uranium (U) contamination in the deep vadose zone (VZ) sediments abundant in calcite mineral is a challenging task considering the formation of highly stable and mobile uranyl complexes with carbonate and calcium in pore water composition. There is a concern that uranium contamination in the VZ can serve as a continued source for groundwater pollution, creating a risk to human health and the environment through the groundwater pathway. This requires in-situ remediation of the radionuclide-contaminated VZ to convert soluble U species to low solubility precipitates that are stable in the natural environment.

Injection of reactive gasses (e.g., NH_3) is a promising technology to decrease U mobility in the unsaturated zone without the addition of liquid amendments. The NH_3 injection creates alkaline conditions that can alter the sediment pore water composition due to a release of elements from minerals (via desorption and dissolution) that are present in the sediment. However, it is not known how VZ pore water constituents (Si, Al^{3+}, HCO_3^-, and Ca_2^+) would affect U(VI) removal/precipitation in alkaline conditions.

This study quantified the role of major pore water constituents typically present in the arid and semi-arid environments of the western regions of the U.S and identified solid uranium-bearing phases that could potentially precipitate from solutions approximating pore water compositions after pH manipulations via ammonia gas injections. Triplicate samples were prepared using six Si (5, 50 100, 150, 200, and 250 mM), six HCO_3^- (0, 3, 25, 50, 75, and 100 mM), and two Ca^{2+} (5 and 10 mM) concentrations. The concentration of aluminum and uranium was kept constant at 5 mM and 0.0084 mM, respectively, in all synthetic formulations tested. Results showed that the percentage of U(VI) removal was controlled by the Si/Al molar ratios and Ca^{2+} concentrations. Regardless of the bicarbonate concentration tested, the percentage of U(VI) removed increased as the Si/Al ratios were increased. However, higher Ca concentrations correlated with higher U(VI) removal, ranging between 96%-99%, at low Si/Al ratios. The SEM images of dried precipitates displayed dense amorphous regions high in silica content, where EDS elemental analysis unveiled higher U atomic percentages. The formation of uranyl silicate and carbonate minerals was also predicted by the speciation modeling. XRD analysis revealed the presence of uranyl carbonate mineral phases (andersonite, grimselite); however, uranyl silicates predicted (Na-boltwoodite) were not identified experimentally, possibly due to the amorphous nature of the silica solid phases observed in our experiments.

Key words: uranium, silica, ammonia gas, vadose zone, removal efficiency

1.0 Introduction

The reprocessing of irradiated fuel to produce plutonium for atomic weapons has left about 202,703 kg of uranium (U) contamination in the subsurface at the U.S. Department of Energy's Hanford Site. This U is a potential source of groundwater contamination and a risk to human health and the environment through water uptake from contaminated wells or discharges to surface water. Uranium is a redox-sensitive element and, depending on the oxidation reduction conditions, mainly occurs in two states: hexavalent uranium [U(VI)] and tetravalent uranium [U(IV)]. These oxidation states determine its mobility in unsaturated and saturated natural systems. In oxic conditions, the chemistry of hexavalent uranium is governed by the dioxo cation (UO_2^{2+}) which is highly soluble and mobile and can readily form complexes with a variety of organic and inorganic ligands depending on the aqueous composition (e.g., proton H^+, anions, cations, and organic ligands). In the absence of the most relevant ligands in aqueous solutions, such as CO_3^{2-}, SiO_4^{4-}, and SO_4^{2-}, the speciation of U is dominated by the UO_2^{2+} cation until pH<5. Between pH 6 and 10, the major dissolved uranyl species are uranyl-hydroxides [e.g., $UO_2(OH)_3^-$, $(UO_2)_2OH^{5+}$, and $(UO_2)_3(OH)_7^-$)]. In carbonate-bearing systems, uranyl carbonate complexes [e.g., $UO_2CO_3(OH)_3^-$, $UO_2CO_3(aq)$, $UO_2(CO_3)_2^{2-}$, and $UO_2(CO_3)_3^{4-}$] are the predominant aqueous species and $UO_2(CO_3)_3^{4-}$ dominates the speciation at pH > 9 (Elles and Lee, 1998). In Ca- and carbonate- rich subsurface environments, typical for western U.S. arid and semi-arid regions including the Hanford Site, U(VI) forms highly soluble and stable calcium-uranyl-carbonate complexes [$Ca_2UO_2(CO_3)_3^o(aq)$, $CaUO_2(CO_3)_3^{2-}$] (Bernard, et al. 1996, 2001; Kalmykov and Chopin, 2000). This can explain the high mobility of U in the Hanford vadose zone (VZ) sediments given its low partition coefficient (K_d) value ranging from 0.2 to 4 mL/g (Cantrell et al., 2003; Zachara et al., 2007). In VZ sediments with abundant calcite

and in the presence of complexing anions such as carbonates (CO_3^{2-}) and hydrous silicates ($H_3SiO_4^-$), uranium tends to form uranyl carbonate and uranyl silicate minerals. Uranophane and boltwoodite are the most common uranyl silicate solid phases found in the VZ environment at Hanford (Szecsody et al., 2012; Um et al., 2009; Zachara et al., 2007). In addition, the VZ sediments contain uranyl carbonate solids, liebigite and rutherfordine, that were found at medium to high concentrations (Szecsody et al. 2012). Radionuclides contaminated the deep (80 to 100 m) VZ at the Hanford Site 200 Area, requiring in-situ stabilization to convert aqueous mobile uranyl carbonates to lower solubility precipitates that are stable in the natural environment. Wellman et al. Wellman et al., (2012) investigated U(VI) stabilization through injections of a sodium tripolyphosphate amendment into the saturated sediments which led to formation of sodium uranyl phosphate mineral phases. However, the addition of liquid amendments into the VZ can cause undesirable downward migration of U and co-contaminants, instigating contamination of the underlying aquifer. Injection of reactive gases such as NH_3 to create alkaline conditions in the VZ is an innovative technology aiming to decrease uranium mobility in the unsaturated zone contaminated with radionuclides without the addition of liquid amendments. The injection of a highly soluble ammonia gas to the VZ prompts the formation of NH_4OH following a subsequent increase in pH from 8.0 to about 11.02 for 0.1% NH_3 (~ 0.063 mol/L NH_3 (aq)) and 11.87 (~3.1 mol/L NH_3 (aq)) for 5% NH_3 (Szecsody et al., 2012; Zhong et al., 2015). This manipulation, triggered by the alkaline pH, can significantly alter the sediment pore water composition and greatly enhance the solubility rates of most minerals such as quartz, calcite, feldspar, and iron oxides that are abundantly present in the sediments. Chou and Wollast (1984) suggested that the rate of mineral dissolution may increase by two to three orders of magnitude with an increase in pH from 8 to 12 at 23ºC. The dissolution of minerals at high pH

conditions can induce the release of silica, carbonate, aluminum, calcium and the alkali metals sodium and potassium to the pore water (Zhong et al., 2015). The subsequent decrease in pH to natural conditions would lead to precipitation of U-phases such as Na- or NH_3-boltwoodite or re-precipitation of various silica and aluminosilicate solid phases and calcium carbonates that may incorporate uranium in a process called co-precipitation (Szecsody et al., 2010b; Zhong et al., 2015). Previous laboratory evaluations showed a decrease in U mobility after ammonia gas injection in the low water content sediments (Szecsody et al., 2010a; Zhong et al., 2015). Another possible mechanism contributing to the decrease of uranium mobility after ammonia gas applications is the coating of U-bearing phases by a low solubility non-uranium precipitate such as cancrinite and sodalite (Zhao et al., 2004) or phyllosicates, carbonate and sodalite, as was found in water-saturated systems of uranium- contaminated sites (Qafoku and Icenhower, 2008). The objective of this research was to examine the effect of calcium ions on the removal/precipitation of U(VI) from synthetic pore water (SPW) solutions composed of variable molar ratios of silicon to aluminum in the presence of bicarbonate. The removal of U(VI) from the synthetic solutions treated with NH_3 gas was quantified for six molar ratios of silica to aluminum and prepared in a wide range of bicarbonate and two calcium concentrations. Manipulations with pore water constituencies can simulate the conditions occurring in the subsurface typical for arid and semi-arid environments throughout the western United States and explain changes in the removal of elements through co-precipitation with silica and aluminosilicates. Parallel studies have focused on the detailed characterization of the uranium-bearing precipitates created after ammonia gas injection.

2.0 Material and methods

Batch experiments were performed to evaluate the effect of Ca^{2+} ions on the removal of uranium from SPW solutions amended with variable Si/Al molar ratio concentrations following NH_3 gas injections. Detailed physical mineralogical and geochemical analysis of Hanford Site VZ soil and porewater compositions that provided concentrations of major cations, anions, alkalinity and pH was reported in a previous study (Serne et al., 2008). For the purpose of this study, the complicated pore water composition was simplified to contain five major components in the SPW: silica, aluminum, uranium, calcium, and bicarbonate with the counter ions, Na^+, K^+, NO_3^-, and Cl^-. The range of Si concentrations was chosen based on previous studies by limiting Si concentrations to a maximum of 250 mM (7.0 g L^{-1}) (Katsenovich et al., 2016; Qafoku et al., 2004; Szecsody et al., 2010b, 2012; Zhong et al., 2015). The aluminum concentration was kept constant at 5 mM, which is slightly higher than was observed in the batch experiments conducted by Zhong et al. (Zhong et al., 2015), and both Si and Al concentrations were orders of magnitude greater than uranium. CO_3^- and HCO_3^- are the major anions in pore water compositions due to the abundance of calcite in Hanford sediments (Qafoku and Icenhower, 2008; Serne et al., 2008). To cover the concentration range of elements released to the solution mixture due to the alkaline dissolution of soil minerals, SPW compositions were formulated with six Si (5, 50 100, 150, 200, and 250 mM), six HCO_3^- (0, 3, 25, 50, 75, and 100 mM), and two Ca^{2+} (5 and 10 mM) concentrations. The concentration of U was kept constant at 0.084 mM (2 mg/L) in all synthetic formulations tested. The experimental results provided a complete range of data for U(VI) removal in the presence of 5 mM of Al across all Si and HCO_3^- concentrations tested in addition to Ca ions commonly present in the pore water composition. Details on the SPW compositions and chemicals used for the formulations are provided in the supporting information (Tables 1S and 2S).

2.1 Sample preparation procedures

Stock solutions of Al (50 mM), Si (420 mM), HCO_3^- (400 mM), and Ca (500 mM) were prepared in deionized water (DIW) by dissolving $Al(NO_3)_3 \cdot 9H_2O$, $Na_2SiO_3 \cdot 9H_20$, $KHCO_3$ and $CaCl_2 \cdot 6H_2O$ salts individually in 50-mL vials. The 100 µg/mL uranyl stock solution was prepared fresh in DIW from the 1000 µg/mL uranyl nitrate stock (SPEX CertiPrep™). Sample preparation procedures at different molar ratios of Si/Al followed the same methods as described in Katsenovich et al., (2016) by mixing the appropriate volume of stock solutions and injecting NH_3 gas (0.1% NH_3 in 99.9% N_2) through 20 µm pores of a metal gas sparger (Mott Corporation) until the pH of the solutions reached a value of ~11 (0.063 mol/L (aq)). Synthetic pore water samples of 5 mL prepared in triplicate were extracted from NH_3-laden aluminum-silicate-carbonate test solutions into 15-mL polyethylene tubes and mixing rapidly with an aliquot from the $CaCl_2$ stock (50 and 100 µL) depending on the targeted Ca concentration (5 mM or 10 mM) in the mixture. The resulting mixture was then spiked with uranium to yield an overall concentration within a solution matrix of 2 mg/L. The final pH of the prepared samples was in the range of 10.9-11.1 (Orion Versa Star pH Benchtop Meter and Orion Double Junction pH Electrode). Control samples were prepared in DIW amended with U(VI) at the same concentration of 2 mg/L to test for U(VI) losses due to sorption to tube walls and caps (Figure 1S). All experimental and control tubes were vortexed and kept in an incubator/shaker at 100 rpm and 25°C. After two days, the tubes were centrifuged for 15 minutes at 4000 rpm (Thermo Scientific, Corvall ST 16R centrifuge) and supernatant solutions were withdrawn to analyze for U(VI), Si, Al, Ca, and inorganic carbon (IC). Preliminary experiments showed that the removal efficiency of U(VI) reached a plateau after two days of agitation on the shaker.

In total, two sets were prepared with a total of 72 triplicate samples amended with 5 mM or 10 mM of Ca in the solution mixtures for all Si/Al molar ratios (1, 10, 20, 30, 40, and 50). For each Si/Al ratio, samples were prepared at six bicarbonate concentrations (0, 3, 25, 50, 75, and 100 mM) as shown in Table 3S (supporting information).

2.2 Analytical Procedures

After centrifugation, an aliquot of supernatant was extracted from each test vial, acidified, and then analyzed for U(VI) via a kinetic phosphorescence analyzer (KPA-11, Chemchek). In addition, the concentrations of Si, Al, and Ca were analyzed via inductively coupled plasma emission spectroscopy (ICP-OES, Perkin Elmer, Optima 7300 DV). In addition, the accuracy of the initial Al, Si, and Ca stock solution concentrations were tested with ICP-OES. For better precision, the concentration of elements was analyzed using different dilutions factors. For analysis with KPA, an aliquot was extracted from the supernatant of each test sample and diluted with 1% HNO_3 between 5 to 100 times. For analysis with the ICP-OES, an extracted aliquot was diluted with DIW in conical polypropylene tubes between 100 to 200 times. The IC of the supernatant solutions was analyzed using a Shimadzu TOC analyzer with an autosampler (TOC-V CSH). Each analysis was repeated until the standard deviation was less than 3%.

2.3 Geochemical Speciation Modeling

The speciation modeling to predict the distribution of uranyl aqueous species and formation of uranium solid phases likely to be present in tested SPW was performed using the Geochemist Workbench (GWB) version 10.0.04 with the Visual MINTEQ database (thermo-minteq) formatted by Jon Petter Gustafsson (KTH Royal Institute of Technology). This database was manually updated with the most recently published thermodynamic equilibrium constants for aqueous complexation reactions for some uranyl species relevant to this study (Grenthe et al.,

1992; Kalmykov and Choppin, 2000; Bernhard et al., 2001; Guillaumont et al., 2003; Guillaumont and Mompean, 2003; Dong and Brooks, 2006; Gorman-Lewis et al., 2008; Richter et al., 2015).

The calcite mineral is abundant in Hanford soil and it exists as a mineralogical component in all subsurface sediments, resulting in dissolved carbonate and calcium ions being common components in the pore and groundwater systems. Therefore, thermodynamic parameters of relevant calcium uranyl silicate, calcium uranyl carbonate, and calcium uranyl oxide hydrate phases were included in the modified database.

The updated thermo-minteq database used for this study also included the stability constants for ternary complexes of uranyl carbonate with alkaline earth metals, $Ca_2UO_2(CO_3)_3(aq)$ and $CaUO_2(CO_3)_3^{2-}$, which play an important role in the aqueous speciation of uranium (Bernhard et al., 1996; Dong and Brooks, 2006; Guillaumont et al., 2003; Kalmykov and Choppin, 2000). These species, along with mixed polynuclear U(VI) hydroxide-carbonate complexes, were updated based on the recommendations from the Thermodynamic Reference Database THEREDA (Richter et al., 2015) (Table 1).

Table 1: Selected uranium aqueous complexation reactions and formation constants (T=25°C, I=0).

Reactions	Log K	Reference
Hydrolysis		
$UO_2OH^+ + H^+ = UO_2^{2+} + H_2O$	-5.25	Guillaumont et al, 2003; Gorman-Lewis et al, 2008; Richter et al, 2015.
$UO_2(OH)_{2\,(aq)} + 2H^+ = UO_2^{2+} + 3H_2O$	-12.15	
$UO_2(OH)_3^- + 3H^+ = UO_2^{2+} + 2H_2O$	-20.25	
$UO_2(OH)_4^{2-} + 4H^+ = UO_2^{2+} + 4H_2O$	-32.40	
$(UO_2)_2(OH)_2^{2+} + 2H+ = 2UO_2^{2+} + 2H_2O$	-5.620	
$(UO_2)_2OH^{3+} + H^+ = 2UO_2^{2+} + H_2O$	-2.700	
$(UO_2)_3(OH)_4^{2+} + 4H^+ = 3UO_2^{2+} + 4H_2O$	-11.90	
$(UO_2)_3(OH)_5^+ + 5H^+ = 3UO_2^{2+} + 5H_2O$	-15.55	
$(UO_2)_4(OH)_7^+ + 7H^+ = 4UO_2^{2} + 7H_2O$	-21.90	
$(UO_2)_3(OH)_7^- + 7H^+ = 3UO_2^{2} + 7H_2O$	-32.2	

Carbonates		
$UO_2^{2+} + CO_3^{2-} = UO_2^{2+} + CO_3^{2-}$	9.94	Guillaumont et al, 2003; Gorman-Lewis et al, 2008; Richter et al, 2015.
$(UO_2)_3(CO_3)_6^{6-} = 3UO_2^{2+} + 6CO_3^{2-}$	54.00	
$(UO_2)(CO_3)_3^{5-} = UO_2^{2+} + 3CO_3^{2-}$	7.19	
$UO_2(CO_3)_2^{2-} = UO_2^{2+} + 2CO_3^{2-}$	16.61	
$UO_2(CO_3)_3^{4-} = UO_2^{2+} + 3CO_3^{2-}$	21.84	
$(UO_2)_3CO_3(OH)_3^{+} + 3H^{+} = 3UO_2^{2+} + CO_3^{2-\ +} + 3H_2O$	0.66	
$(UO_2)_2CO_3(OH)_3^{-} + 3\,H^{+} = 2UO_2^{2+} + CO_3^{2-} + 3H_2O$	-0.86	
$Ca_2UO_2(CO_3)_3\ (aq) = UO_2^{2+} + 3CO_3^{2-\ +} + 2Ca^{2+}$	30.60	Dong and Brooks, 2006; Gorman-Lewis et al, 2008; Richter et al, 2015.
$Ca\ UO_2(CO_3)_3^{2-} = UO_2^{2+} + 3CO_3^{2-\ +} + Ca^{2+}$	27.18	
$U(CO_3)_4^{4-} = UO^{4+} + 4CO_3^{2-} + H_2O$	35.22	Guillaumont et al, 2003; Thoenen et al, 2014.
$U(CO_3)_5^{6-} = UO^{4+} + 5CO_3^{2-}$	33.90	
$(UO_2)_{11}(CO_3)_6(OH)_{12}^{2-} + 12H+ = 11UO_2^{2+} + 6\ CO_3^{2-} + 12\ H_2O$	36.42	Guillaumont et al, 2003; Richter et al, 2015.
Silicates, chlorine, and nitrate		
$UO_2^{2+} + H_4SiO_4$	-1.84	Guillaumont et al, 2003; Gorman-Lewis et al, 2008; Richter et al, 2015.
$UO_2NO_3^{+} = NO_3^{-} + UO_2^{2+}$	-0.300	Guillaumont et al, 2003; Richter et al, 2015; Thoenen et al, 2014.
$UO_2Cl^{+} = Cl^{-} + UO_2^{2+}$	0.17	
$UO_2Cl_2\ (aq)^{+} = 2Cl^{-} + UO_2^{2+}$	-1.100	

The $Ca_2UO_2(CO_3)_3$(aq) complex was reported as a major U(VI) aqueous species in the Hanford Site vadose zone porewater (Liu et al., 2004); so, it was important to evaluate its presence in the synthetic pore water compositions.

Previous studies on uranium conducted in Si-rich solutions have demonstrated the formation of uranyl-silicate minerals (Wronkiewicz et. al., 1996). Uranyl silicates, boltwoodite and uranophane were also found in the Hanford Site VZ sediments (Catalano et al., 2004; Um et al., 2009).Thus, thermodynamic parameters to predict uranium solubility from relevant uranyl silicate minerals (Na,K), boltwoodite [$(Na,K)(UO_2)(H_4SiO_4)\cdot 0.5H_2O$], and uranophane [$Ca(UO_2)_2(HSiO_4)_2\cdot 5H_2O$], uranyl carbonate minerals like grimselite [$NaK_3UO_2(CO_3)_3$], rutherfordine [UO_2CO_3], liebigite [$Ca_2UO_2(CO_3)_3\cdot 10H_2O$(cr)], andersonite

207 $[Na_2CaUO_2(CO_3)_3{\cdot}6H_2O]$, cejkaite $[Na_4UO_2(CO_3)_3]$ as well as uranyl oxide hydrate solid phases
208 such as becquerelite $[Ca_2(UO_2)_6{\cdot}18H_2O]$, clarkeite $[Na(UO_2){\cdot}2H_2O]$, compreignacite
209 $[K_2(UO_2)_6{\cdot}18H_2O]$, and metaschoepite $[UO_3(H_2O)_2]$), were included or modified in the thermo-
210 minteq database used for speciation calculations in this study (Grenthe et al., 2004; Gorman-
211 Lewis et al., 2008; Shvareva et al., 2011; Richter et al., 2015). In addition, metaschoepite in the
212 updated thermo-minteq database replaced the schoepite species based on its similarity to the
213 schoepite species (Guillaumont et al., 2003; Gorman-Lewis et al., 2008; Shvareva et al., 2011)
214 (Table 2).

215 **Table 2. Uranyl mineral phases used in the speciation modeling**

Mineral Phase	Structural Formula	Log K_{sp}	Reference
Uranyl Carbonates			
Andersonite	$Na_2CaUO_2(CO_3)_36H_2O$	-37.50	Alwan & Williams, Mineral. Mag. (1980) cited in Gorman-Lewis et al, 2008.
Cejkaite	$Na_4UO_2(CO_3)_3$	-27.18	THEREDA database (Richter 2015)
Grimselite	$NaK_3UO_2(CO3)_3H_2O$	-37.10	Gorman-Lewis et al, 2008.
Liebigite	$Ca_2UO_2(CO_3)_310H_2O$	-36.90	Gorman-Lewis et al, 2008.
Rutherfordine	UO_2CO_3	-14.46	This phase is present in the original thermo-minteq
Uranyl hydroxides			
Becquerelite	$Ca\ (UO_2)_6\ O_4(OH)_6(H_2O)_8$	40.50	Gorman-Lewis et.al (2008), suggested value from OECD NEA. Confirmed by Richter et al, 2015 (THEREDA database)
Clarkeite	$Na(UO_2)O(OH)$	9.400	Gorman-Lewis JCT (2008), THEREDA Richter et al, 2015
Metaschoepite	$(UO_2)_8O_2(OH)_{12}(H_2O)_{10}$	5.350	Gorman-Lewis (2008) review and THEREDA database (Richter et al, 2015)
Uranyl Silicates			
Soddyite	$(UO_2)_2H_4SiO_4\ 2H_2O$	6.090	Gorman-Lewis (2008) review and THEREDA (Richter et al, 2015
K-Boltwoodite	$KH_4SiO_4\ UO_2\ 1.5H_2O$	4.120	Shrevena et al, 2011 and THEREDA database (Richter et al, 2015)
Na-Boltwoodite	$NaHSiO_4\ UO_2\ 1.5H_2O$	6.070	Gorman-Lewis et al, (2008); Richter et al, 2015; Shrevena et al, 2011
Uranophane	$Ca(UO_2)_2(HSiO_4)_2\ 5H_2O$	10.82	Gorman-Lewis et al, (2008) and Log Ksp modified with Shrevena et al, 2011; confirmed by Richter et al, 2015.

216

217 The simulated porewater compositions included five cations and four anions as well as the
218 counter ions. Concentrations of uranium, aluminum, and silica were kept constant in all
219 modeling simulations at 0.0084 mM, 5 mM, and 50 mM, respectively. In addition, simulations to

predict the aqueous speciation and the formation of solid phases were conducted using two calcium concentrations (5 and 10 mM) combined with three bicarbonate concentrations [bicarbonate-free (0 mM), "low" (3 mM) and "high" (50 mM)]. Dissolved oxygen (DO) was set at 8.4 mg/L at a constant temperature of 25^{o}C. In the GWB Reactants pane, experimental conditions were simulated by sliding pH from 8 to 11.02 for 0.1% of NH_3 (0.063 mol/L of NH_3(aq)). The simulations were repeated by sliding pH from 8 to 11.87, imitating the pH values reached after the injection of 5% of NH_3 (5% NH_3 in 95% N_2; 3.1 mol/L of NH_3 (aq)). The NH_3(aq) concentrations were assumed to be at equilibrium in the solutions. The speciation modeling was performed for a system closed to the exchange of CO_2 with the atmosphere, which is more applicable to the core of the ammonia gas injection in the field. In addition, speciation modeling assumed that ammonia would not reduce U(VI) to U(IV) (Katsenovich et. al., 2016). The process of uranium reduction by ammonia is strongly impeded by: the presence of air, which is 21% oxygen, in the headspace of capped vials; the addition of nitrate ions with the uranyl standard prepared in 2% nitric acid and pH adjustment solutions; and by the stabilizing effect of bicarbonate in the bicarbonate-amended solutions due to the formation of uranyl-carbonate complexes (Campbell et al., 2015). Based on these assumptions, the aqueous U(IV) species were not considered in this study. The uranium aqueous species and saturation indexes (SI) of mineral phases were calculated and graphed as a function of pH.

It should be noted that the thermodynamic data of uranium solid and liquid species is still under review and investigation (Altmaier et al., 2013; Gorman-Lewis 2008) and the solubility calculations and uranium speciation are based on current knowledge, but may have significant associated uncertainty.

2.4 Mineral Characterization

The mineralogical and morphological characteristics of the dried uranium-bearing precipitates were analyzed using scanning electron microscope-energy dispersive spectroscopy (SEM-EDS) and powder X-ray diffraction (XRD). The samples' surface composition and the development of crystalline structures were monitored by means of SEM-EDS. These measurements, collectively with analytical results and thermodynamic speciation modeling data, allowed for identification of the U(VI) solid phases present in multicomponent precipitates. The sample preparation procedures for these studies were similar to uranium removal experiments with the difference being that the former deals with the dried solid precipitate. Experimental samples for XRD and SEM-EDS analysis were prepared with the addition of 50 mM of Si, 5 mM of Al, 5 mM and 10 mM of Ca, and 400 ppm of U(VI) in the mixture solution using "high" (50 mM HCO_3) and "low" (3 mM HCO_3) concentrations of bicarbonate. The increase in uranium concentration helped to enhance the atomic percentage of U(VI) in the sample composition and improved U detection. Two solutions containing 3 mM and 50 mM of HCO_3^- were prepared in 50-mL vials and then combined with the appropriate concentrations of Na_2SiO_3 and $Al(NO_3)_3$ (Table 1S). These relatively alkaline solutions were adjusted to a pH of 8 using concentrated nitric acid to better mimic the natural conditions of the Hanford 200 Area VZ (Szecsody et al., 2012). Then the solutions were sparged with ammonia gas (NH_3) to increase pH up to 11 and 10-mL aliquots from the ammonia-laden solutions were dispensed into 15-mL sample vials. Lastly, the solutions were finished by the addition of $CaCl_2$ and uranyl stocks (Table 1S), using volumes less than 100 µL to minimally effect the concentrations of the other components in the mixture. The solutions were left for 2 weeks at 25^{o}C and then centrifuged for 15 minutes at 4000 rpm and the

supernatant was carefully decanted and reserved for uranium analysis via KPA while the solids were dried in an oven at 30°C for two weeks in preparation for SEM-EDS and XRD analysis.

Electron microscopy was performed using a JEOL-5910-LV with accelerative potentials between 10 kV and 20 kV. Dried samples were sputter-coated with a thin layer of gold/palladium using an SPI-Module Control and Sputter unit. EDS analysis was accomplished using an EDAX Sapphire detector with UTW Window paired with Genesis software. Micrographs were prepared in both secondary electron (SE) and backscatter secondary electron (BSE) modes with the objective lens aperture 2 at 30 µm diameter and the spot sizes (condenser lens) ranging from 35-40".

X-ray diffraction analyses were performed at 35 kV and 40 mA via a Bruker 5000D XRD instrument. Diffraction patterns were obtained using a copper Cu Kα radiation source (λ=0.154056 nm) with a tungsten filter. The XRD was programmed to run over a 2-theta (2θ) range from 5° to 70° with a 0.02° step size and 3 second counting per step. Dry samples were carefully ground into a fine powder using a mortar and pestle under the fume hood. Then, the pulverized sample was packed into the small recess of a plastic sample holder that was designed specifically for the small amount of sample available. Two method blanks, prepared identically to the experimental sample with the exception of uranium, were also ground and analyzed. Identification of the uranyl mineral phases was based on a comparison of the XRD patterns measured for the selected precipitate samples with the mineral powder diffraction files (PDF) published by the American Mineralogist Crystal Structure Database (Downs and Hall-Wallace, 2003).

3.0 Results and Discussions

3.1 The Effect of Ca Ions on the Removal of U(VI)

The experimental results were evaluated based on the percent removal of the elements of interest: U(VI), Si, Al, Ca, and IC. Figure 1 depicts the percent removal of these elements in solutions with pH increased up to 11 as a result of NH_3 gas injection.

The removal of U(VI) involves a phenomenon of Si precipitation following trapping of U by the co-precipitation process (Allard et al., 1999). It is known that dissolved silica polymerizes in Si-rich alkaline solutions. This process involves nucleation reactions and the formation of amorphous silica particles by polymerization of $Si(OH)_4$ (Iler 1979). Nucleation reactions can be accelerated by aluminosilicate impurities serving as "seeds" due to a reaction between monomeric silica $Si(OH)_4$ and $Al(OH)_3$ (Iler, 1979).

$$> SiOH + Al(OH)_3^+ \leftrightarrow \quad > SiOAl(OH)_2 + H^+ \qquad [1]$$

In addition, amorphous Si precipitates can be formed by the aggregation of colloidal particles due to the coagulation of alkaline earth metal carbonates (Kellermeier et al., 2010; Voinescu et al., 2007). The additions of divalent ions such as calcium are commonly used for coagulation of colloidal silica from water; they flocculate colloidal silica along with other suspended or precipitated matter (Sheikholeslami and Bright, 2002).

Our previous studies suggest that in Ca-free solutions, higher concentrations of Si, Al and bicarbonate tend to have greater removal efficiencies of U(VI), up to 95-99% at Si concentrations between 150 mM and 250 mM. However, the process of U(VI) removal was not as efficient when the concentration of Si was less than 50 mM (Si/Al ratio between 1 and 10). Overall, the formation of amorphous Si always correlated with the removal of U(VI), Si, and Al from the solution. When there was only a small decrease in Si concentrations from the

supernatant solutions, the removal of U(VI) was diminutive or not observed (Katsenovich et al., 2016).

The findings of a current study indicate that the percentage of U(VI) removal was largely controlled by the Si/Al ratios and calcium concentrations (Figure 1 (A,B)). Furthermore, regardless of the bicarbonate concentration tested, the percent of U(VI) removed increased as the Si/Al ratios were increased. The uranium removed varied between 87% - 100%, starting at a Si/Al ratio of 10 for all bicarbonate concentrations tested. The higher Ca concentration correlated with higher U(VI) removal, ranging between 96%-99% at low Si/Al ratios ≤10. Possible mechanisms responsible for the U(VI) removal include the cumulative effect of nucleation reactions forming calcium carbonate clusters upon mixing $CaCl_2$ and Na_2CO_3 and then uptake of uranyl by co-precipitation with calcium carbonate (Reeder et al., 2000; Reeder et al., 2001). The following deposition of hydrated amorphous silica layers on the precipitated calcium carbonate grains creates a silica layer coating on the aggregates (Kellermeier et al., 2010; Klein and Walter, 1995; Voinescu et al., 2007). Previous studies on U(VI) trapping in natural Si/Al-rich gels were consistent with a co-precipitation process of U, Si and Al that discussed encapsulation of U(VI) within a silicate polymer (Allard et al., 1999).

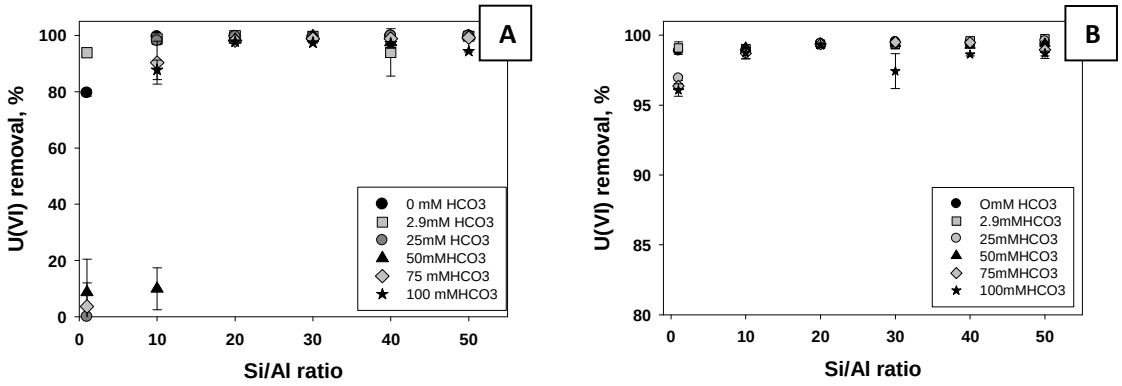

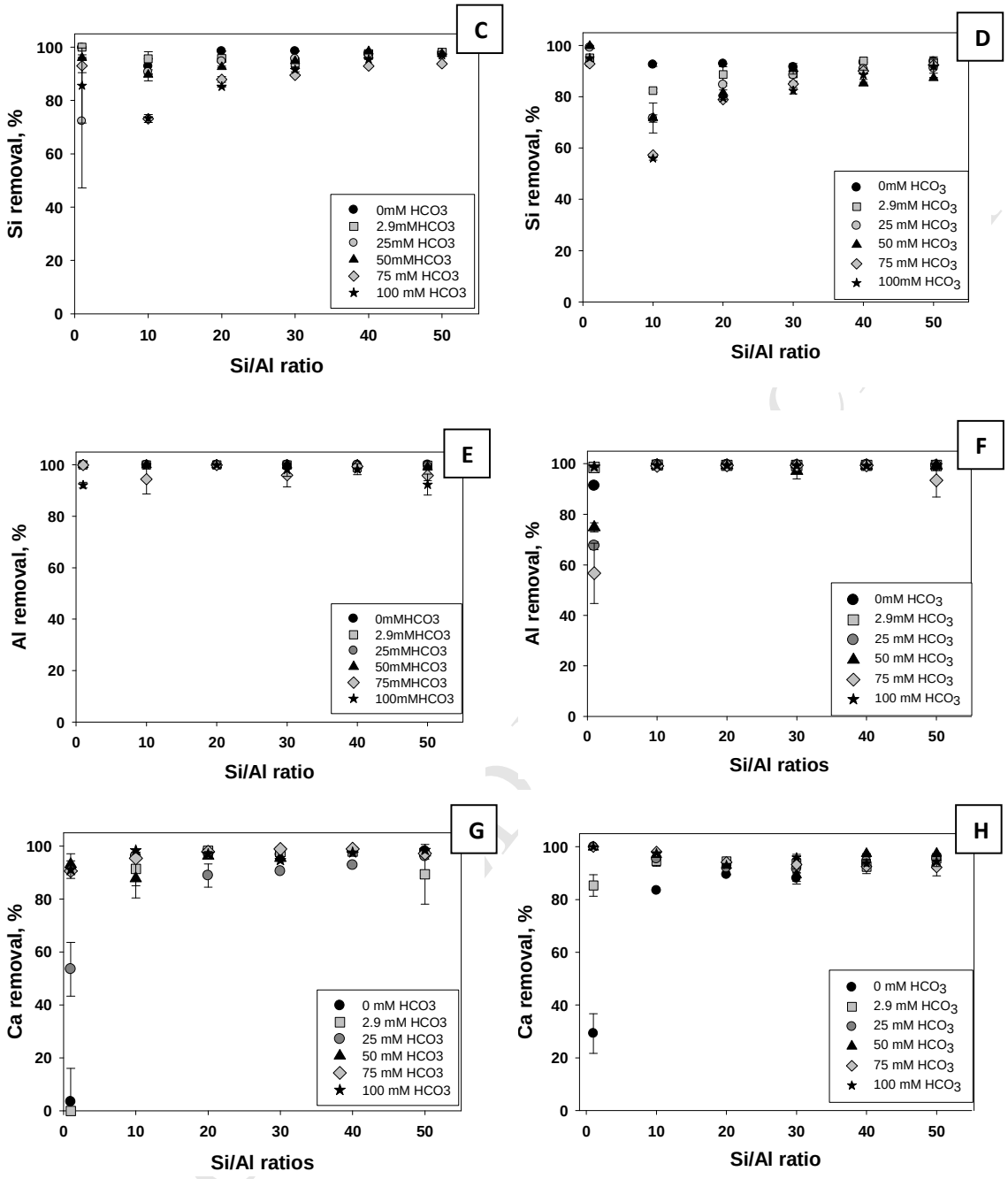

Figure 1. Removal of U(VI) from the solution mixture prepared with 5 mM of Ca (A) and 10 mM of Ca (B); Removal of Si from the solution mixture prepared with 5 mM of Ca (C) and 10 mM Ca (D); Removal of Al from the solution mixture prepared with 5 mM of Ca (E) and 10 mM Ca (F); Removal of Ca from the solution mixture prepared with 5 mM of Ca (G) and 10 mM of Ca (H).

329 The low solubility calcium carbonates may evolve from the synthetic solutions amended with
330 bicarbonate, calcium and silica at high pH values between 10 and 11. According to Kellermeier
331 et al. (2010), at alkaline pH, precipitation of the amorphous calcium carbonate in Si-rich
332 solutions induces dissociation of bicarbonate and the release of protons resulting in a local
333 decrease in pH near the growing carbonate phases:

334 $$HCO_3^- \leftrightarrow CO_3^{2-} + H^+ \xrightarrow{Ca^{2+}} CaCO_3 \downarrow \quad [2]$$

335 Silicate species respond to these local pH changes by polymerization reactions followed by
336 particle aggregation and flocculation (Iler, 1979; Kellermeier et al., 2010):

337 $$Si-O^- + H^+ \leftrightarrow -SiOH + HO-Si \xrightarrow{-H_2O} Si-O-Si \rightarrow SiO_2 \downarrow \quad [3]$$

338 Therefore, the decrease in pH caused by the precipitation of carbonate increases the local
339 supersaturation of silicic acid in the surroundings of the growing carbonate phases, thus
340 provoking precipitation of silica (García-Ruiz et al., 2009).
341 When a soluble silicate is mixed with solutions containing metals other than the alkali metal
342 group, insoluble amorphous metal silicates along with other elements are precipitated out of
343 solution (Iler, 1979). Iler (Iler, 1975) proposed mechanisms of silica coagulation by calcium ions
344 leading to precipitation of those elements from solution. The adsorption of a calcium ion on the
345 negatively charged silica surface liberates only one hydrogen ion by ion exchange, thus creating
346 one additional negative site on the Si surface (Iler, 1975). This negative site is neutralized by one
347 adsorbed calcium ion that retains a single positive charge.

348 $$Ca^{2+} + Si <^{OH}_{OH} \rightarrow H^+ + Si <^{OH}_{O-Ca^{2+}} \quad [4]$$

349 Iler (1975) assumed that a possible mechanism of Si coagulation is through interparticle bonding
350 that involves bridging by positively charged calcium ions and attraction between surfaces

bearing a mosaic of positive and negative sites. The equilibrium distribution of dissolved aqueous and solid phase species is discussed later in the text.

The removal of silica concentrations from the tested solutions indicated that, in bicarbonate-free and 3 mM HCO_3 solution mixtures amended with 5 mM of Ca, the percentage of silica removal at Si/Al ratios of 1 and 10 remained between 97% - 99%; however, Si removal was lowered to 73% at higher bicarbonate concentrations ranging from 25 to 100 mM (Figure 1C). At higher Si/Al ratios greater than 10, the percentage of Si removal was found between 89% and 99% for all bicarbonate solution concentrations tested.

When the Ca concentration was increased up to 10 mM, the percentage of silica removal at Si/Al ratio 1, the lowest ratio investigated in this study, was increased to 93-99%. The precipitates formed after combining all stock solutions are usually not homogeneous in composition. This depends on the degree of Si polymerization and precipitation reactions that occur in the solution mixture. This causes some discrepancies in the results between replicate samples, especially those prepared for low Si/Al ratios (Figure 1D).

In all experiments, the removal of Si correlated with the removal of U(VI) from solutions. Yet, at the lowest Si/Al ratio, over 70% of the Si was removed from solution for all bicarbonate concentrations, but less than 10% of the U was removed for the highest bicarbonate concentrations. However, as Si concentration was increased, the effect of carbonate complexing becomes minimal. This result demonstrates the effect of carbonate complexing on uranium removal by silica. The opposite happened in experiments with Ca-free solutions; data demonstrated higher U(VI) removal from the supernatant as the concentration of bicarbonate solutions was increased (Katsenovich et al., 2016).

373 The unique chemical affinity between silicon and aluminum is responsible for the removal of
374 aluminum from the solution (Figure 1E, F). Monomeric silica, $Si(OH)_4$, reacts with Al^{3+} ions to
375 form aluminum silicate, which tends to precipitate (Iler, 1979). According to Iler (1979), SiO_2
376 surfaces exposed to solutions containing aluminum form aluminosilicate surface complexes by
377 reaction with the following stoichiometry:

378 $$2Si(OH)_4 + 2Al^{3+} + H_2O = \quad Al_2Si_2O_5(OH)_4 + 6H^+ \qquad [5]$$

379 The presence of aluminum can radically affect the amorphous silica surface properties due to
380 formation of aluminosilicate surface complexes that results in an entire armored surface coating,
381 which is extensive enough to reverse the net negative Si surface charge to positive (Dove and
382 Rimstidt, 1994). Iler (1979) also demonstrated that low aluminum concentrations can give a
383 significant reduction in solubility for silica gel.

384 The removal of Ca^{2+} ions from the solution is apparently due to the precipitation of calcium
385 carbonate and silica coagulation reactions initiated upon addition of Ca^{2+} ions (Figure 1G, H).
386 So, the addition of $CaCl_2$ to the SPW solution mixture containing sodium silicate and bicarbonate
387 ions influences silica coagulation reactions with the formation of Si-based multicomponent
388 precipitates, which could retain co-precipitated uranium (as U silicate or/and carbonate) within
389 its amorphous structure.

390 Another possible mechanism for Ca removal from the solution mixture is the adsorption of Ca
391 ions on the silica amorphous surface. The adsorption of a divalent cation on the surface of
392 amorphous silica may increase the development of positive charge sites, making a bridge by
393 reacting with two particles at their point of contact. The adsorption of metal ions on the silica
394 surface may also affect the surface properties and, in addition, displace H^+ into the solution
395 (Dove and Rimstidt, 1994; Iler, 1975):

396 $$SiOH + Ca^{2+} \rightarrow SiOCa^{+} + H^{+}$$ [6]

397 Kellermeier et al. (2012) examined the formation of cluster-like species grown when alkaline-
398 earth carbonates and silica are co-precipitated at elevated pH. In their experiments, silica was
399 coagulated by the addition of $CaCl_2$. Analyses of the flocculated material showed that it
400 essentially consisted of amorphous silica, with minor amounts of calcium entrapped between the
401 coagulated particles. They ruled out precipitation of calcium-rich silica particles in the samples
402 and expected that the major fraction of the Ca^{2+} ions to be free and available for interaction with
403 carbonate under the experimental conditions.

404 According to the speciation modeling predictions, carbonate ions at pH 10-11 are mainly
405 distributed between CO_3^{2-}, HCO_3^{-}, $CaCO_3$, $CaHCO_3^{+}$ and $NaCO_3^{-}$ species. From those species,
406 only the precipitation of calcium carbonate can control the removal of inorganic carbon from the
407 aqueous solution. Speciation modeling suggested that at pH 11, the percent of total calcium
408 carbonate species accounts 0.03% for 3 mM HCO_3 and 0.1% at 10 mM of Ca and 50 mM HCO_3
409 of the total concentration of bicarbonate present initially in the solutions. However, experimental
410 results suggested that the removal of inorganic carbon was much higher and increased for 10
411 mM of Ca in the solution mixture composition, up to 80-86% for the 25-100 mM range of HCO_3^{-}
412 . For the compositions prepared with 5 mM of Ca, the removal of inorganic carbon at Si/Al ratios
413 ranging from 30 to 50 averaged 35-45%, which is also much higher than the values predicted by
414 GWB (Figure 4S, 5S) . We hypothesized that the discrepancies between GWB-predicted percent
415 of CO_3^{2-} precipitation as calcium carbonate and the percent of IC removal obtained in the
416 experiments were due to silica coagulation leading to encapsulation of carbonate-bearing solids
417 within an amorphous silicate matrix. Precipitation of $CaCO_3$ and its encapsulation within
418 amorphous Si-bearing precipitates causes changes in the carbonate system due to the decrease in

the calcium carbonate saturation state. Coating by silica may force a shift in the equilibrium between bicarbonate ions towards generation of $CaCO_3$, which precipitates out of solution. In previous studies, silica uptake onto calcium carbonate was shown to increase in higher-ionic-strength solutions and higher silica aqueous concentrations (Kitano et al., 1979). The reaction continues with carbonate solid phases, most likely via hydroxyl groups, a mechanism that provokes silica flocculation (Ruiz, 1998).

3.2 Speciation modeling results

Modeling calculations on uranium species distribution showed similar results for both calcium concentrations tested (Figure 2 for 10 mM of Ca and Figure 2S for 5 mM of Ca). According to speciation modeling predictions, in bicarbonate–free SPW solutions, $UO_2(OH)_3^-$ and $UO_2(OH)_4^{2-}$ were the predominant uranyl species. However, these concentrations were ~44% lower than reported for Ca- and bicarbonate-free SPW solutions (Katsenovich et al., 2016). In the aqueous solution containing carbonate ions at pH > 8, U(VI) species are mostly present as $UO_2(CO_3)_3^{4-}$, but the addition of calcium ions changed the speciation towards the formation of $Ca_2UO_2(CO_3)_3(aq)$ and $CaUO_2(CO_3)_3^{2-}$ for 0.1% NH_3. Concentrations of $Ca_2UO_2(CO_3)_3(aq)$, $CaUO_2(CO_3)_3^{2-}$, and $UO_2(OH)_3^-$ decreased at higher bicarbonate concentrations but stabilized after pH 10.5. At 3 mM of bicarbonate, these complexes were noted to decrease considerably starting at pH 9.0 for 5 mM of Ca (not shown) and pH>8.5 for 10 mM of Ca (Figure 2B1). At higher bicarbonate concentrations, $UO_2(CO_3)_3^{4-}$ was the dominant uranyl species and its concentration was almost unchanged over the studied pH range followed by the $CaUO_2(CO_3)_3^{2-}$ species (Figure 2C1).

The speciation modeling (SM) predicted the formation of relevant uranium mineral phases; in the bicarbonate-free conditions, speciation predicted the formation of uranophane (SI=1). It also

identified the formation of Na-boltwoodite and undersaturated uranyl oxide hydrates, clarkeite and metaschopite; the last two were favorable under bicarbonate-free and low bicarbonate concentrations (Figure 2 A2). At low bicarbonate concentration at pH close to 9, most uranyl solid phases were undersaturated except uranyl silicate minerals, (Na-K) boltwoodite with SI at 0.94 and uranophane as\t 1 (Figure 2B2). At high bicarbonate concentration, grimselite was found to be the main uranyl –bearing solid phase in the pH range from 8.0 to 11 (Figure 2 A2, B2). Similar speciation modeling results were obtained for the formulation that included 5 mM of Ca.

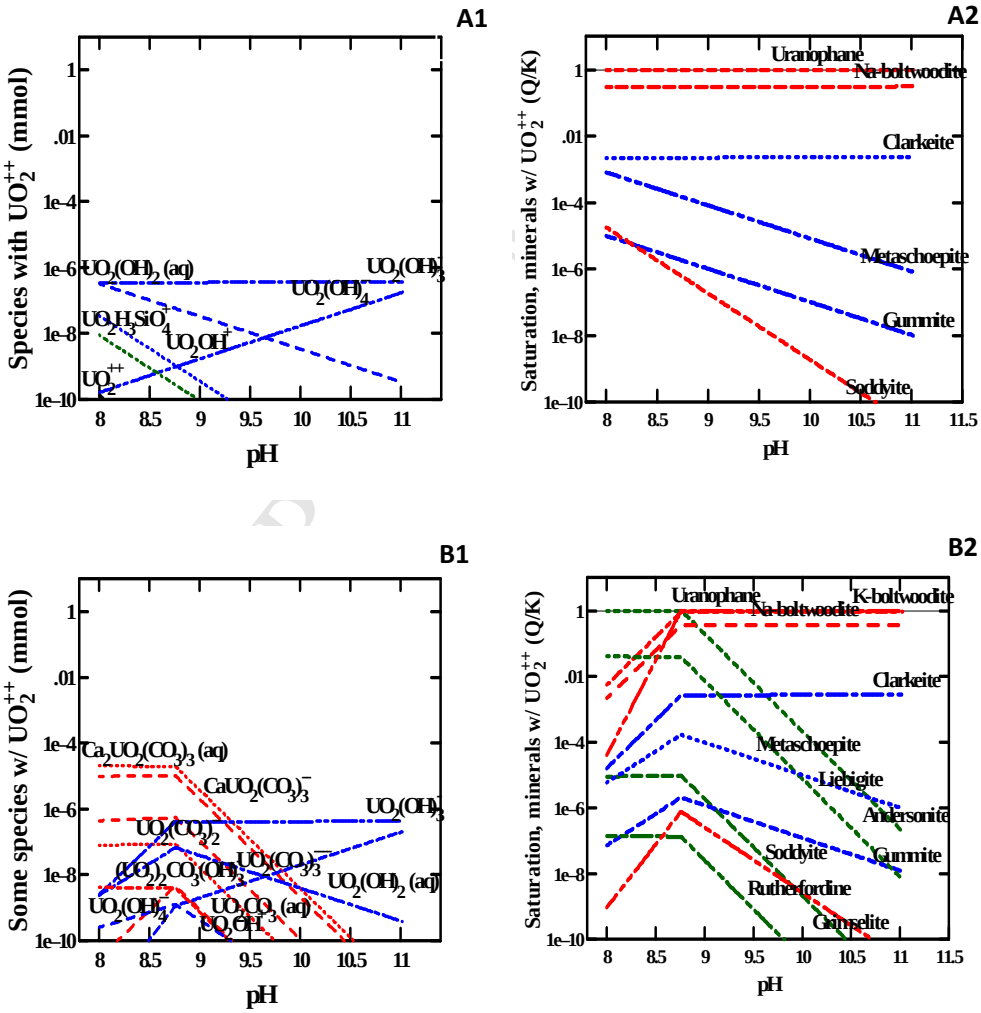

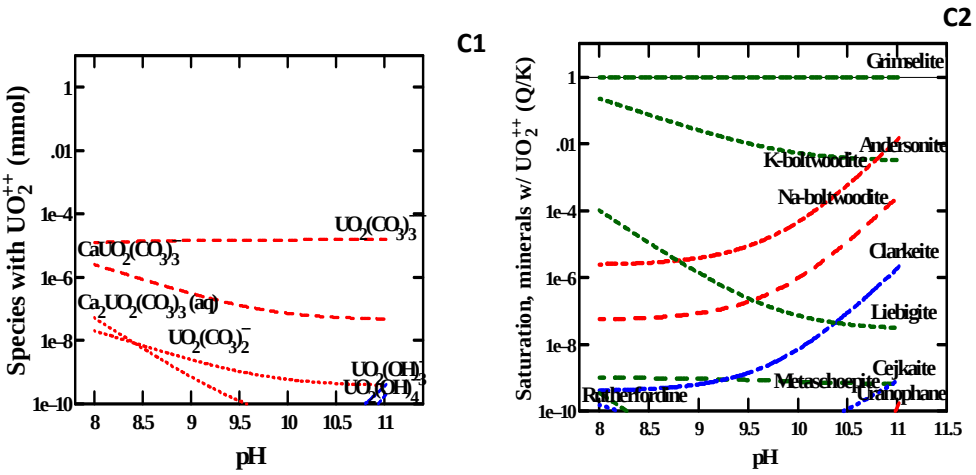

Figure 2. Diagrams of uranium aqueous species and saturation indices of some of uranium-bearing mineral phases plotted as a function of pH for 0.1% of NH_3 [0.063 mol/L NH_3(aq)]. Sample composition includes 10 mM of Ca, 50 mM of Si and varied HCO_3^- concentrations. The first row shows diagrams for HCO_3-free samples (A1, A2), the 2nd and 3rd rows show the diagrams for 3.0 mM (B1, B2) and 50 mM of HCO_3^- (C1, C2).

3.3 Characterization of uranyl solid phases

Studies also attempted to determine the morphological and mineralogical characteristics of the uranium solid phases produced during ammonia treatment. SEM-EDS analyses were performed for observation of uranium phases (Figure 3) and to select representative samples for XRD analysis (Figure 4). The samples prepared with "high" bicarbonate concentrations showed the uranium dense regions of amorphous collection. EDS analysis of these areas resulted in uranium atomic percentages of 14.8% (Figure 3A). The diffraction analysis revealed potential matches for grimselite ($K_3Na(UO_2)(CO_3)_3 \cdot H_2O$), along with calcite and the overwhelming presence of nitratine ($NaNO_3$) (pure mineral intensity is not shown on the graph) (Figure 4A). The finding of grimselite mineral in the sample composition matches the speciation modeling results conducted for "high" bicarbonate samples.

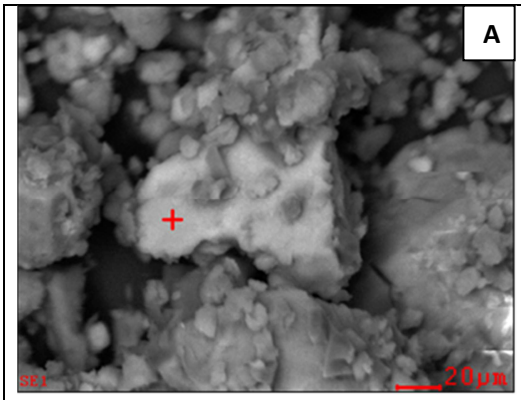

Element	Wt%	At%
CK	08.24	15.18
NK	04.13	06.53
OK	32.78	45.37
NaK	08.81	08.48
AlK	02.19	01.80
SiK	20.51	16.17
ClK	04.57	02.85
KK	01.53	00.87
CaK	02.46	01.36
UL	14.78	01.37
Matrix	Correction	ZAF

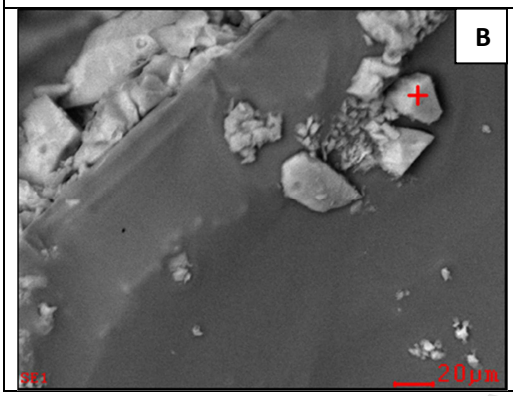

Element	Wt%	At%
CK	14.60	31.53
OK	10.80	17.50
NaK	02.51	02.83
AlK	02.14	02.05
SiK	21.06	19.45
ClK	12.13	08.87
UM	11.42	01.24
KK	06.10	04.05
CaK	19.26	12.46
Matrix	Correction	ZAF

Figure 3.SEM image of the dried precipitate sample and the spot composition using EDS. A) Sample composition included 50 mM of Si, 5 mM Al, 10 mM of Ca and 50 mM HCO_3. B) Sample composition included 50 mM of Si, 5 mM Al, 10 mM of Ca and 3 mM HCO_3.

The low bicarbonate precipitate composition showed only significant amorphous uranium-dense areas with U atomic percentages at the level of 11% (Figure 3B), which coincided with Si weight percentage at the level of 21%.

The XRD pattern produced a broad undefined single peak between 2Θ between 12 and 22, suggesting the presence in the sample of amorphous materials as well as well-defined peaks representative for crystalline forms (Figure 4B). The presence of boltwoodite and uranophane were predicted by the speciation modeling (Figure 2 A2, B2, C2) and SEM-EDS identified areas of concentrated uranium and Si. However, uranyl silicates were not detected with any certainty by powder XRD perhaps due to the amorphous nature of these solid phases in our experiments.

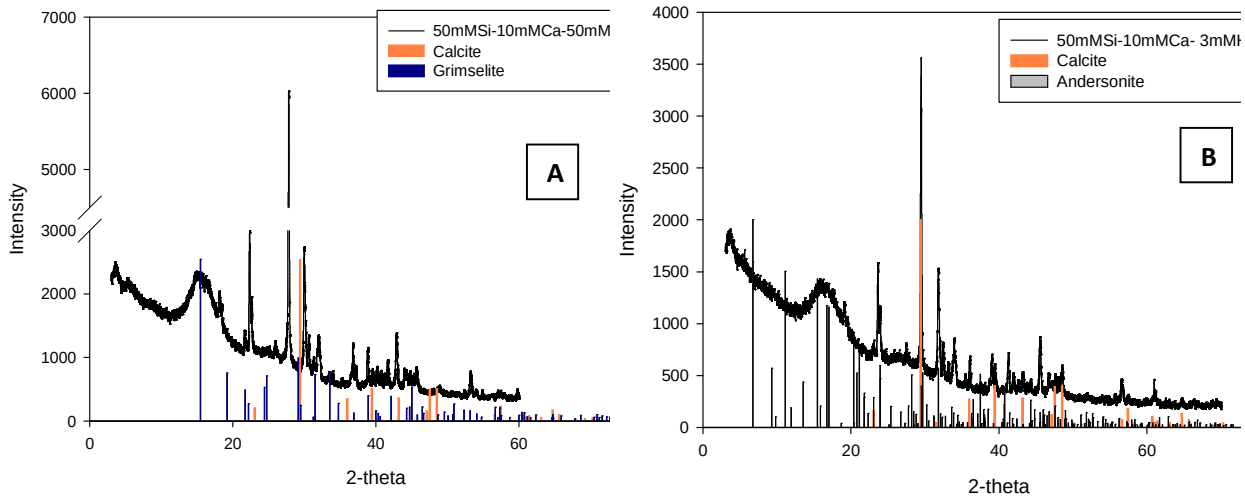

Figure 4. XRD Diffractogram for uranium-bearing precipitate samples prepared with A) 50 mM of Si, 5 mM Al, 10 mM of Ca and 50 mM HCO_3. (left y-axis intensity of the sample and right-y-side reference pattern); B) 50 mM of Si, 5 mM Al, 15 mM of Ca and 3 mM HCO_3.

4.0 Conclusion

Our results provided details on the effect of various Si/Al ratios as well as bicarbonate and calcium concentrations on the removal of uranium from the synthetic sediment-free solution mixtures. It is evident that solutions with higher concentrations of Si and Ca exhibited greater removal efficiencies of U(VI), reaching up to 98-99%. In the presence of 10 mM of Ca, the removal of U(VI) have overshadowed the results obtained for 5 mM of Ca ions introduced in the solution mixture. In addition, when the Ca concentration was increased up to 10 mM, the percentage of silica removal at Si:Al ratio 1, the lowest ratio investigated in this study, was increased to 93-99%, which was higher than the results obtained in the presence of 5 mM of Ca. In all of the experiments, the removal of Si correlated with the removal of U(VI) from solution. Overall, the formation of precipitate always correlated with the removal of U(VI), Si, Al and Ca from the solution. GWB modeling predicted that the U(VI) was present in solution dominantly as $Ca_2UO_2(CO_3)_3$ and $CaUO_2(CO_3)_3^{-2}$. In the presence of Ca, the speciation modeling predicted supersaturation of uranophane, (Na-K) boltwoodite and grimselite phases, indicating that these

minerals can be precipitated during the treatment with ammonia gas. XRD analysis revealed the formation of grimselite in the samples prepared with high bicarbonate concentrations of 50 mM. At low bicarbonate concentrations, XRD detected the formation of andersonite phases. XRD analyses haven't identified uranyl silicate phases; however, SEM-EDS suggested that higher Si weight percentage coincided with higher U wt%, which could justify the formation of uranyl silicate minerals predicted by speciation modeling calculations.

5.0 Acknowledgements

Funding for this research was provided by the U.S. Department of Energy, Office of Environmental Management, under Cooperative Agreement DE-EM0000598. The authors also acknowledge Ms. Peggy Shoffner for her excellent comments and suggestions.

References

Allard, T., Ildefonse, P., Beaucaire, C., Calas, G., 1999. Structural chemistry of uranium associated with Si, Al, Fe gels in a granitic uranium mine. Chemical Geology, 158(1): 81-103.

Altmaier, M., X. Gaona and T. Fanghanel, 2013. Recent advances in aqueous actinide chemistry and thermodynamics. Chem Rev 113(2): 901-943.

Bernhard, G., Geipel, G., Brendler, V., Nitsche, H., 1996. Speciation of uranium in seepage waters of a mine tailing pile studied by time-resolved laser-induced fluorescence spectroscopy (TRLFS). Radiochimica Acta, 74(s1): 87-92.

Bernhard, G. et al., 2001. Uranyl (VI) carbonate complex formation: Validation of the Ca2UO2 (CO3) 3 (aq.) species. Radiochimica Acta International journal for chemical aspects of nuclear science and technology, 89(8/2001): 511.

Campbell, K.M., Gallegos, T.J., Landa, E.R., 2015. Biogeochemical aspects of uranium mineralization, mining, milling, and remediation. Applied Geochemistry, 57: 206-235.

Cantrell, K.J., Last, G.V., JEFFREY, R., 2003. Hanford contaminant distribution coefficient database and users guide. United States. Department of Energy.

Catalano, J.G., Heald, S.M., Zachara, J.M., Brown, G.E., 2004. Spectroscopic and diffraction study of uranium speciation in contaminated vadose zone sediments from the Hanford Site, Washington State. Environmental science & technology, 38(10): 2822-2828.

Chou, L., Wollast, R., 1984. Study of the weathering of albite at room temperature and pressure with a fluidized bed reactor. Geochimica et Cosmochimica Acta, 48(11): 2205-2217.

529 Dong, W. and Brooks, S.C., 2006. Determination of the formation constants of ternary
530 complexes of uranyl and carbonate with alkaline earth metals (Mg2+, Ca2+, Sr2+, and
531 Ba2+) using anion exchange method. Environmental Science & Technology, 40(15):
532 4689-4695.

533 Dove, P., Rimstidt, J., 1994. Silica-water interactions. Reviews in Mineralogy and Geochemistry,
534 29(1): 259-308.

535 Downs, R.T., Hall-Wallace, M., 2003. The American Mineralogist crystal structure database.
536 American Mineralogist, 88(1): 247-250.

537 García-Ruiz, J.M., Melero-García, E., Hyde, S.T., 2009. Morphogenesis of self-assembled
538 nanocrystalline materials of barium carbonate and silica. Science, 323(5912): 362-365.

539 Gorman-Lewis, D., Burns, P.C., Fein, J.B., 2008. Review of uranyl mineral solubility
540 measurements. The Journal of Chemical Thermodynamics, 40(3): 335-352.

541 Grenthe, I. et al., 1992. Chemical thermodynamics of uranium, 1. North-Holland Amsterdam.

542 Grenthe, I. et al., 2004. Chemical thermodynamics of uranium. North-Holland Amsterdam.

543 Guillaumont, R. et al., 2003. Update on the chemical thermodynamics of U, Np, Pu, Am and Tc.
544 Chemical Thermodynamics, 5.

545 Guillaumont, R., Mompean, F.J., 2003. Update on the chemical thermodynamics of uranium,
546 neptunium, plutonium, americium and technetium.

547 Hummel, W., Berner, U., Curti, E., Pearson, F., & Thoenen, T. (2014). PSI/Nagra Chemical
548 Thermodynamic Database 12/07. Paul Scherrer Institut, Villigen PSI, Switzerland:
549 Nuclear Energy and Safety Research Department Laboratory for Waste Management
550 (LES).

551 Iler, R.K., 1975. Coagulation of colloidal silica by calcium ions, mechanism, and effect of
552 particle size. Journal of Colloid and Interface Science, 53(3): 476-488.

553 Iler, R.K., 1979. The chemistry of silica: solubility, polymerization, colloid and surface
554 properties, and biochemistry. Canada: John Wiley &Sons Inc.

555 Kalmykov, S.N., Choppin, G.R., 2000. Mixed $Ca^{2+}/UO_2^{2+}/CO_3^{2-}$ complex formation at different
556 ionic strengths. Radiochimica Acta International journal for chemical aspects of nuclear
557 science and technology, 88(9-11/2000): 603.

558 Katsenovich, Y.P., Cardona, C., Lapierre, R., Szecsody, J., Lagos, L.E., 2016. The effect of Si
559 and Al concentrations on the removal of U (VI) in the alkaline conditions created by NH
560 3 gas. Applied Geochemistry, 73: 109-117.

561 Kellermeier, M. et al., 2012. Colloidal stabilization of calcium carbonate prenucleation clusters
562 with silica. Advanced Functional Materials, 22(20): 4301-4311.

563 Kellermeier, M. et al., 2010. Stabilization of amorphous calcium carbonate in inorganic silica-
564 rich environments. Journal of the American Chemical Society, 132(50): 17859-17866.

565 Kitano, Y., Okumura, M., Idogaki, M., 1979. Behavior of dissolved silica in parent solution at
566 the formation of calcium carbonate. Geochemical Journal, 13(6): 253-260.

567 Klein, R.T., Walter, L.M., 1995. Interactions between dissolved silica and carbonate minerals:
568 An experimental study at 25–50 C. Chemical geology, 125(1): 29-43.

569 Liu, C. et al., 2004. Dissolution of uranyl microprecipitates in subsurface sediments at Hanford
570 Site, USA. Geochimica et Cosmochimica Acta, 68(22): 4519-4537.

571 Qafoku, N.P., Icenhower, J.P., 2008. Interactions of aqueous U (VI) with soil minerals in slightly
572 alkaline natural systems. Reviews in Environmental Science and Bio/Technology, 7(4):
573 355-380.

574 Reeder, R.J., Nugent, M., Lamble, G.M., Tait, C.D., Morris, D.E., 2000. Uranyl incorporation
575 into calcite and aragonite: XAFS and luminescence studies. Environmental Science &
576 Technology, 34(4): 638-644.

577 Reeder, R.J. et al., 2001. Coprecipitation of uranium (VI) with calcite: XAFS, micro-XAS, and
578 luminescence characterization. Geochimica et Cosmochimica Acta, 65(20): 3491-3503.

579 Richter, A., Bok, F., & Brendler, V. (2015). Data compilation and evaluation for U(IV) and
580 U(VI) for the thermodynamic reference database THEREDA. (No. HZDR-065). Dresden:
581 Helmholtz Zentrum Dresden - Rossendorf.

582 Ruiz, J.M.G., 1998. Carbonate precipitation into alkaline silica-rich environments. Geology,
583 26(9): 843-846.

584 Serne, R.J. et al., 2008. Characterization of vadose zone sediment: Borehole 299-E33-45 near
585 BX-102 in the B-BX-BY waste management area, Pacific Northwest National Laboratory
586 (PNNL), Richland, WA (US).

587 Sheikholeslami, R., Bright, J., 2002. Silica and metals removal by pretreatment to prevent
588 fouling of reverse osmosis membranes. Desalination, 143(3): 255-267.

589 Shvareva, T.Y. et al., 2011. Thermodynamic characterization of boltwoodite and uranophane:
590 Enthalpy of formation and aqueous solubility. Geochimica et Cosmochimica Acta,
591 75(18): 5269-5282.

592 Szecsody, J.E. et al., 2010a. Remediation of Uranium in the Hanford Vadose Zone Using
593 Ammonia Gas: FY 2010 Laboratory-Scale Experiments PNNL-20004. Pac. Northw.Natl.
594 Lab., Richland, WA. PNNL-20004; Other: 20899; 830403000; TRN: US1103124 United
595 States10.2172/1006311Other: 20899; 830403000; TRN: US1103124Thu Jul 21 07:12:49
596 EDT 2011PNNLEnglish.

597 Szecsody, J.E. et al., 2010b. Remediation of Uranium in the Hanford Vadose Zone Using Gas-
598 Transported Reactants: Laboratory-Scale Experiments. PNNL-18879, Pacific Northwest
599 National Laboratory, Richland, Washington. Accessed December, 15: 2010.

600 Szecsody, J.E. et al., 2012. Geochemical and Geophysical Changes during Ammonia Gas
601 Treatment of Vadose Zone Sediments for Uranium Remediation. Vadose Zone Journal:
602 1-13.

603 Thoenen, T., Hummel, W., Berner, U., Curti, E., 2014. The PSI/Nagra Chemical
604 Thermodynamic Database 12/07. National Energy and Safety Research Department
605 Laboratory for Waste Management (LES), Cooperative for the Disposal of Radioactive.
606 Paul Scherrer Institut, Villigen PSI, Switzerland.

607 Um, W. et al., 2009. Uranium phases in contaminated sediments below Hanford's U tank farm.
608 Environmental science & technology, 43(12): 4280-4286.

609 Voinescu, A.E. et al., 2007. Co-precipitation of silica and alkaline-earth carbonates using TEOS
610 as silica source. Journal of crystal growth, 306(1): 152-158.

611 Wellman, D.M., Freshley, M.D., Johnson, T.C., Miracle, A.L., 2012. Contaminants in Vadose
612 Zone Environments. Vadose Zone Journal, 11(4).

613 Wronkiewicz, D. J., J. K. Bates, S. F. Wolf & E. C. Buck (1996) Ten-year results from
614 unsaturated drip tests with UO 2 at 90 C: implications for the corrosion of spent nuclear
615 fuel. Journal of Nuclear Materials, 238, 78-95.

616 Zachara, J.M. et al., 2007. A site-wide perspective on uranium geochemistry at the Hanford Site.

617 Zhao, H., Deng, Y., Harsh, J.B., Flury, M., Boyle, J.S., 2004. Alteration of kaolinite to cancrinite
618 and sodalite by simulated Hanford tank waste and its impact on cesium retention. Clays
619 and Clay Minerals, 52(1): 1-13.

620 Zhong, L., Szecsody, J.E., Truex, M.J., Williams, M.D., Liu, Y., 2015. Ammonia gas transport
621 and reactions in unsaturated sediments: Implications for use as an amendment to
622 immobilize inorganic contaminants. Journal of Hazardous Materials, 289: 118-129.

623

624

625

626

627

628

629

630

631

632

633

634

635

Percentage of U(VI) removal was controlled by the Si/Al ratios and Ca concentrations.

Higher calcium concentrations correlated with higher U(VI) removal.

Speciation modeling predicted the formation of relevant uranium mineral phases.

Precipitation correlated with the removal of U(VI), Si, Al and Ca from solution.